Neutron diffraction study of the peritectic growth of the $Al_{65}Cu_{20}Fe_{15}$ icosahedral quasi-crystal

1990 J. Phys.: Condens. Matter 2 6339

(http://iopscience.iop.org/0953-8984/2/30/001)

J. Phys.: Condens. Matter **2** (1990) 6339–6360. Printed in the UK

Neutron diffraction study of the peritectic growth of the $Al_{65}Cu_{20}Fe_{15}$ icosahedral quasi-crystal

C Dong†§, J M Dubois†, M de Boissieu‡‖ and C Janot‡

† Laboratoire de Science et Génie des Matériaux Métalliques (CNRS URA 159), Ecole des Mines, Parc de Saurupt, F-54042 Nancy Cédex, France

‡ Institut Laue Langevin, BP156X, F-38042 Grenoble Cédex, France

Received 23 February 1990

Abstract. This paper reports a thorough description of the phase transformations taking place in the $Al_{65}Cu_{20}Fe_{15}$ ingot and melt-spun samples during heating and cooling runs as recorded by neutron diffraction. Upon cooling, the icosahedral phase is found to form in a peritectic reaction involving θ-$Al_{13}Fe_4$, a BCC phase of approximate composition Al_7Cu_2Fe and liquid. Its isothermal growth mechanism is discussed. There are some indications that the so-called stable and perfect icosahedral phase is not a truly equilibrium phase at room temperature. In the case of the melt-spun sample, upon heating, the T-Al_7Cu_2Fe phase participates in the transformations concerning the icosahedral phase.

1. Introduction

As it is supposed to be a room-temperature stable quasi-crystal of $m\bar{3}5$ point group symmetry, the icosahedral phase (I phase) in $Al_{65}Cu_{20}Fe_{15}$ alloy raises hopes of revealing many mysteries concerning the physical, chemical and metallurgical aspects of quasi-crystalline materials, and has been the focus of quasi-crystal research since its discovery by Tsai *et al* [1]. In a previous paper [2], we have described the phase transformations taking place during continuous cooling of this alloy from the liquid temperature to the temperature when the I phase has fully grown. Our results showed that for this specific composition, the I phase grows in a peritectic reaction involving a residual liquid phase (the L phase) and the monoclinic θ-$Al_{13}Fe_4$ phase (the θ phase), in contrast with other stable quasi-crystals, which grow directly from the melt [3–5].

In recent months, two companion crystalline phases of the I phase have been discovered. A BCC cubic phase takes part in the peritectic growth process, on the one hand, and a rhombohedral microcrystalline material forms below 650 °C, on the other [6]. This latter compound gives a powder diffraction pattern closely resembling the one of the icosahedral phase, and its formation at low temperature means that the I phase is not a stable phase at room temperature. Thus, there is a need for a more detailed examination of the phase transformations occurring before and after the formation of the icosahedral phase in Al–Cu–Fe alloys. To this end, we present in this paper a detailed account of the results of our real-time neutron diffraction study of the phase transformations taking

§ Also at Institut Laue–Langevin, Grenoble, France.

‖ Present address: LTPCM, BP75, F-38402 St Martin D'Heres, France.

0953-8984/90/306339 + 22 $03.50

place in the $Al_{65}Cu_{20}Fe_{15}$ alloy. The peritectic reaction, in equilibrium with the residual liquid, is further analysed [2]. The reversibility of the transition upon heating and cooling, as well as the isothermal transformation mechanism, is investigated. Comparison is also made between a bulk master ingot, solidified from liquid during conventional casting, and a melt-spun sample.

2. Crystallographic background

The nominal composition of the I phase has been found in the close vicinity of $Al_{64}Cu_{24}Fe_{12}$ by several authors. This icosahedral phase exhibits a unique peculiarity in that it exhibits a FCC ordering (F lattice) in six-dimensional real space (6D) as indicated by superstructure diffraction lines, which appear in addition to the conventional pattern already observed with the Al–Mn icosahedral phase. The reciprocal space of the I phase is spanned by a BCC I lattice [7]. In fact, the intensity of the I lattice extra nodes, indexed by N, M principal indices (defined in [8]) with N odd, depends significantly on the thermal history of the sample. This strongly suggests [9] that the FCC 6D real-space superstructure is the result of some chemical ordering, or of periodically repeated variants of the decoration of the odd and even nodes of the primitive 6D cubic lattice of the conventional 6D icosahedral lattice. In the following, we shall refer to the diffraction lines of the I phase according to letters [10] for the sake of simplification. The correspondence between letters [10], principal indices N, M and full indexing [8] is given in table 1 for the diffraction peaks of relevance to the present study. The position of each line at temperature 1070 K is also reported, corresponding to a 6D cubic lattice parameter $a_6 = 6.43$ Å. Note that the E ($N = 7, M = 11$), G ($N = 11, M = 16$) and N ($N = 27, M = 43$) lines have N odd, but only the E line has a sufficiently large intensity, which will indicate hereafter the F superstructure.

Furthermore, the same alloy shows two coexisting crystalline phases that were discovered since the date of submission of our paper [2] and still need to be fully determined. The first is the rhombohedral microcrystalline approximant phase pointed out by Audier and Guyot [6] in slowly cooled specimens. The lattice parameters are $a = 32.08$ Å, $\gamma = 36°$. Because of the low resolution of the detector used in the present study (see next section), this crystalline phase cannot easily be distinguished from the I phase,

Table 1. Letter labels [10] and indexings [8] of the principal diffraction lines of the I phase at 1070 K.

Line	N, M	Full indexing	$Q = 4\pi \sin\theta/\lambda$ (Å^{-1})
D	6, 9	120100	1.644
E	7, 11	120011	1.807
F	8, 12	220000	1.901
G	11, 16	130001	2.206
H	14, 21	230010	2.516
K	18, 29	230012	2.928
L	20, 32	240000	3.080
N	27, 43	340011	3.572
O[a]	28, 44	240022	3.623

[a] The O line is not listed in [10].

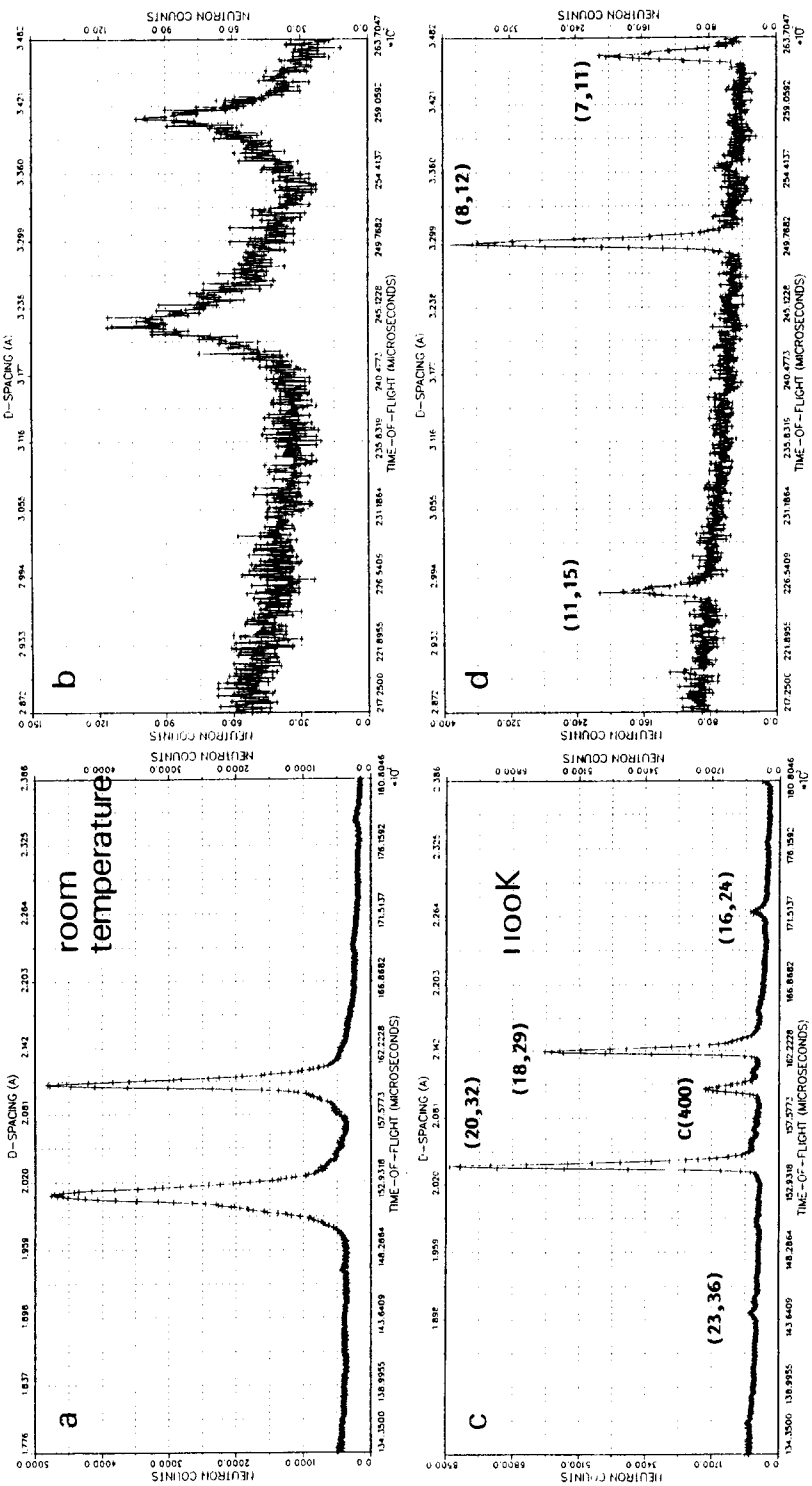

Figure 1. Diffraction line profiles measured on the $Al_{64}Cu_{23}Fe_{13}$ alloy at the Intense Pulsed Neutron Source of Argonne National Laboratory (C Janot, D L Price and J W Richardson Jr). The microcrystalline rhombohedral phase ((*a*), (*b*)) has very broad peaks as compared to the narrow peak of the high-temperature equilibrium icosahedral phase ((*c*), (*d*), $T = 1100\,\mathrm{K}$).

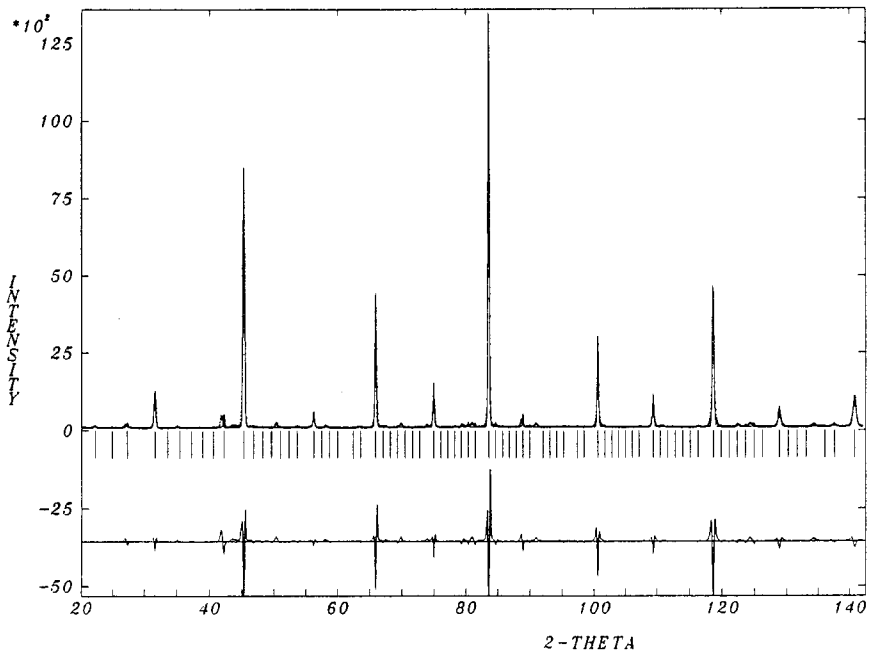

Figure 2. High-resolution neutron diffraction pattern of the cubic phase measured at 4 K on the D2B diffractometer (ILL). The abscissa gives the scattering vector modulus $Q = 4\pi \sin\theta/\lambda$. A 2θ angle scale has been superimposed on this figure for the sake of comparison with the other figures (λ = 1.596 Å).

except for intensity changes and very small shifts of line positions. Such effects are more clearly visible in electron microscopy [11] and x-ray single-crystal [12] studies. High-resolution neutron diffraction studies [13] reveal broadened and asymmetric Bragg peaks in the rhombohedral microcrystalline phase, in contrast to the sharp, symmetric peaks of the I phase. This difference is exemplified in figure 1, which compares a few line profiles measured with a microcrystalline sample at room temperature and with the same sample at 1100 K when the I phase has formed (the details are to be published elsewhere). In the following, primed letters D′, E′, etc, will refer to diffraction peaks of the rhombohedral microcrystalline phase (the R phase) that have positions corresponding to the lines of the I phase.

Another crystalline phase of relevance here is the cubic phase (the C phase), which forms very close to the stoichiometric composition of the I phase. The high-resolution neutron diffraction pattern shown in figure 2, measured at 4 K, requires a cubic lattice parameter as large as 8.28 Å. However, a few weak lines, identifiable on the difference curve between fitted and observed patterns, have not yet been interpreted. This indicates that the chemical ordering of the cubic phase may extend over distances larger than the above lattice parameter. The refinement of the structure is in progress.

3. Experimental procedure

A master alloy of nominal composition $Al_{65}Cu_{20}Fe_{15}$ was prepared by RF melting of the pure elemental metals. The cylindrical ingots so obtained were 1 cm in diameter.

Neutron diffraction was used to study the successive phase transformation as already described in [14]. A time-resolved neutron diffraction experiment was performed on the instrument D1B at the Institut Laue Langevin in Grenoble. We report in this paper on two different experiments. An ingot was placed into a single-crystalline sapphire cell oriented out of its Bragg position (run 1), on the one hand, and powders from melt-spun ribbons in vitreous tubes (run 2), on the other. Each container was located in the diffraction centre of an evacuated furnace and was examined by using a neutron diffractometer with a 400-cell detector covering a Bragg angle range of $2\theta = 80°$. The wavelength used was 2.52 Å. The high neutron flux makes it possible to extract diffraction patterns at 3 min intervals with satisfactory statistics, short enough to record the dynamical phase transformation processes. The furnace is computer-controlled and can heat or cool the sample at constant rate or run at any isothermal plateau of interest. Different heat treatment processes were performed on these two kinds of samples and thereby the I phase transformations during heating as well as its growth during continuous cooling and isothermal annealing have been monitored.

4. Run 1: phase transformations in the $Al_{65}Cu_{20}Fe_{15}$ ingot sample

4.1. Heating process

Figure 3 is the neutron diffraction pattern of the ingot sample before heat treatment. The principal phase present can be indexed according to the scheme indicated in table 1. However, we will show in the following that it was in fact the rhombohedral micro-

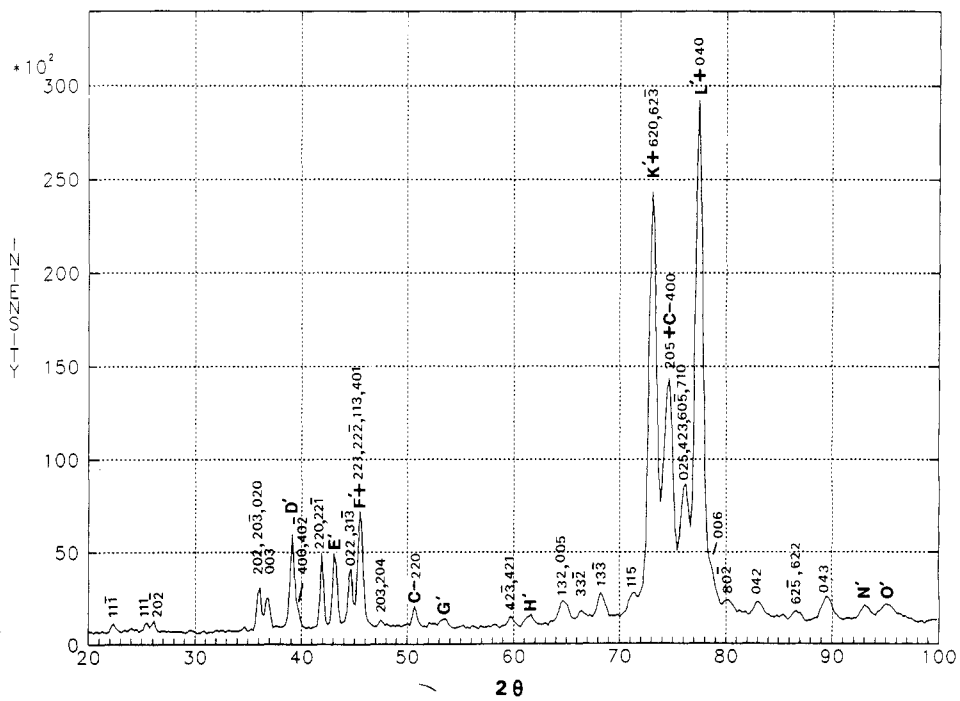

Figure 3. Neutron diffraction pattern of the ingot sample in the as-cast state.

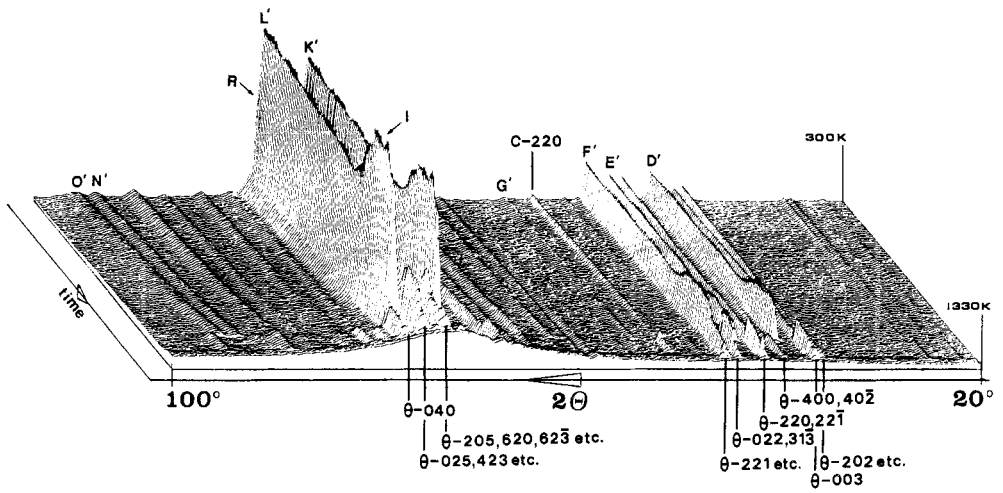

Figure 4. Three-dimensional perspective view of the heating process as recorded by neutron diffraction at 3 min intervals. Note that the θ-(205) and θ-(620, $62\bar{3}$) peaks merge into a single peak near the melting point. (As several heating rates have been used during this heating, it would be too complex to show the corresponding temperature profile).

crystalline phase (the R phase). Indexing the other reflections proves that the monoclinic θ-$Al_{13}Fe_4$ phase [15] and the cubic phase are also present as minor components. An electron microscopy study, performed on a small fraction of the ingot before being heat-treated, confirms these conclusions.

Figure 4 is a three-dimensional view of the evolution of the diffraction patterns (corrected for background intensities) at 3 min intervals upon heating from room temperature to the liquid state at 1330 K. Upon heating from room temperature, the peak amplitudes decrease gradually. This is presumably due to the increasing importance of Debye–Waller factor. At 910 K, the intense peaks begin to rise sharply. This reaction transforms the R phase into the real I phase. The amount of the I phase reaches a maximum at about 1100 K. Above this temperature, the I phase disappears according to the peritectic reaction already mentioned [2]. This process is best illustrated in figure 5 where the intensity of the D peak is plotted as a function of temperature. The role of the other phases during this R → I phase transformation is still not clear because the principal peaks of phases θ and C are hidden behind the I phase peak 'walls' in figure 4. Figure 6 shows enlarged plots of a part of figure 4 where this reaction process is more obvious. Figure 6(*b*) is the view seen from the direction indicated in figure 6(*a*), with the K peak of the I phase being suppressed in order to reveal the peak profiles located behind it. Now we can see that this phase transformation is accompanied by very complex changes of the peak intensities of phases θ and C: the (400) peak of the C phase vanishes whereas the (025) *et al* peaks of the θ phase first rise a little and then fall again, keeping a smooth profile. Such a phenomenon suggests that both the θ and the C phases are strongly involved in the transformation of the R phase to the I phase and makes it a eutectoid reaction according to the formula: R + θ + C → I + θ. The (220) peak of phase C disappears as the above reaction goes on. The non-uniform change of the diffraction intensities of the θ phase also implies an elemental transfer process associated with this eutectoid reaction. Audier *et al* [6] have found the R → I transformation during *in situ* heating of similar samples in a transmission electron microscope, but they did not

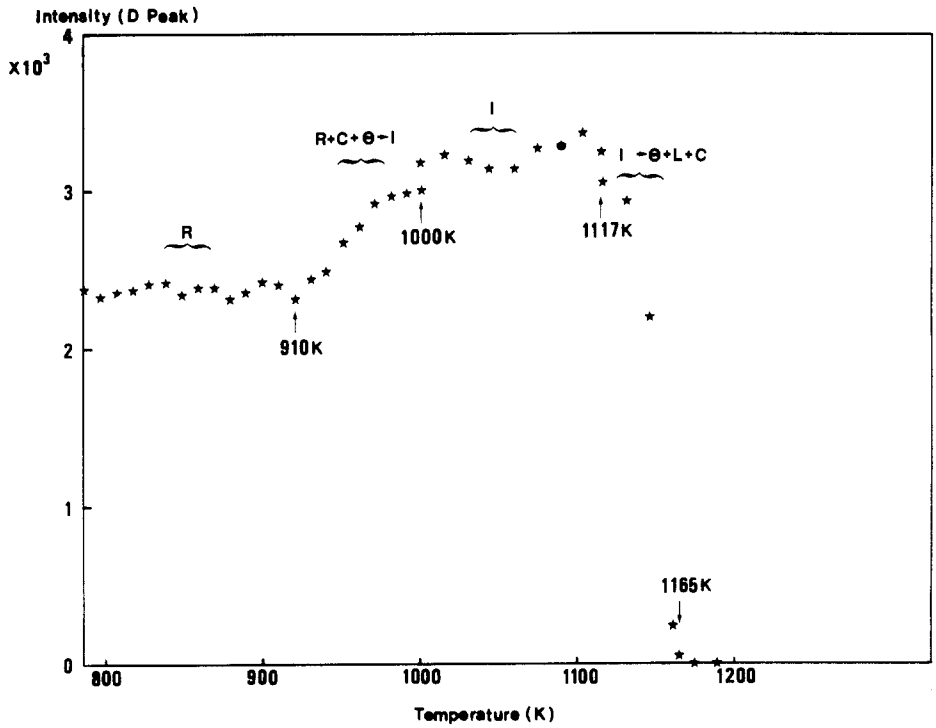

Figure 5. The intensity versus temperature of peak D showing its development during heating.

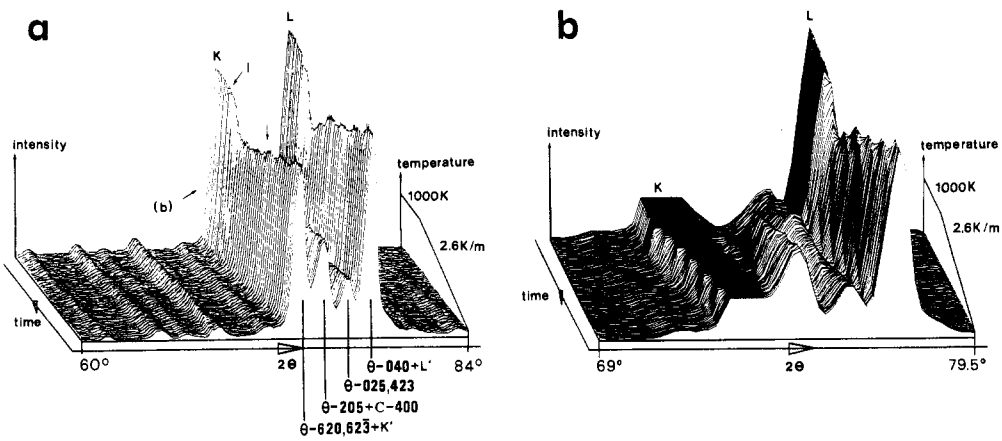

Figure 6. Enlarged plots of the part of figure 4 where the R + θ + C → I + θ reaction is better revealed. The (*b*) plot is the view seen along the direction indicated in (*a*) with peak K being suppressed.

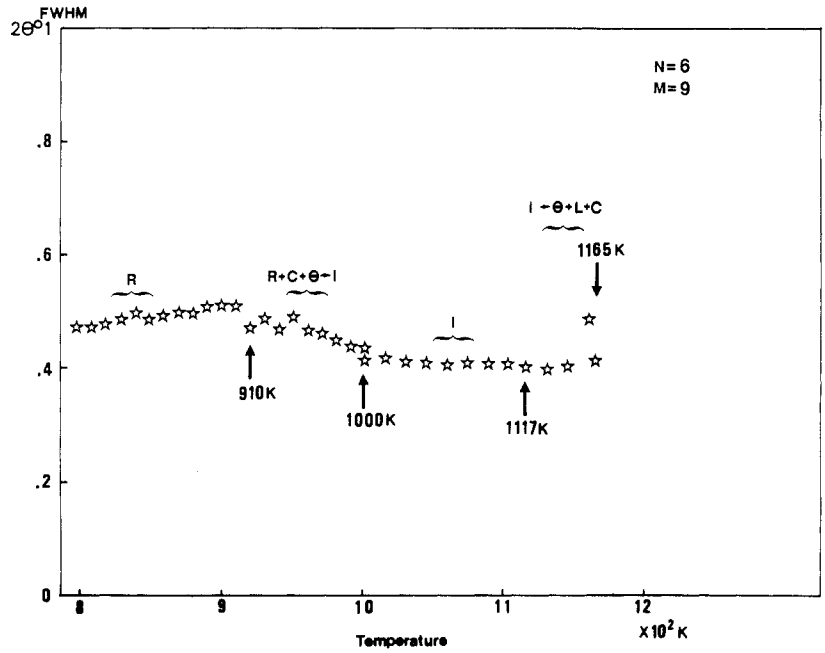

Figure 7. FWHM of peak D of the I phase as a function of heating temperature.

mention any involvement of phases θ or C. Other evidence that supports the R → I transformation is the narrowing of the peaks of the I phase (which reaches the instrumental resolution) as compared to the figures measured with the R phase (figure 7). Several authors have obtained a highly ordered I phase by first annealing a sample at about 1110 K, which is in the stability temperature range of the I phase (see figure 5), then quenching it in water [10] or cooling quickly down to low temperature [7, 16]. Therefore, it is reasonable to believe that what has been assumed to be the perfect I phase is a high-temperature phase.

The second phase transformation begins at 1117 K and ends at 1165 K where the I phase is decomposed into phases θ, C and liquid. Note that the C phase disappears when the I phase grows out and reappears after the I phase is decomposed by peritectic reaction. Such a process is clearly illustrated by the development of C-(220) peak shown in figure 4. This C phase disappears at 1250 K, shortly before the θ phase melts at 1317 K. The last pattern visible in the foreground of the diagram is typical of the liquid state. In short, there exist the following phase transformations during heating from room temperature up to the melting point:

$T = 910$ K, heating rate = 2.6 K min^{-1}	$R + \theta + C \rightarrow I + \theta$
$T = 1117$ K, heating rate = 4.3 K min^{-1}	$I + \theta \rightarrow \theta + C + L$
$T = 1250$ K, heating rate = 4.4 K min^{-1}	$\theta + C + L \rightarrow \theta + L$
$T = 1317$ K, heating rate = 4.4 K min^{-1}	$\theta + L \rightarrow L$.

4.2. Cooling process

Figure 8 is the three-dimensional view that summarises the path upon cooling from liquid

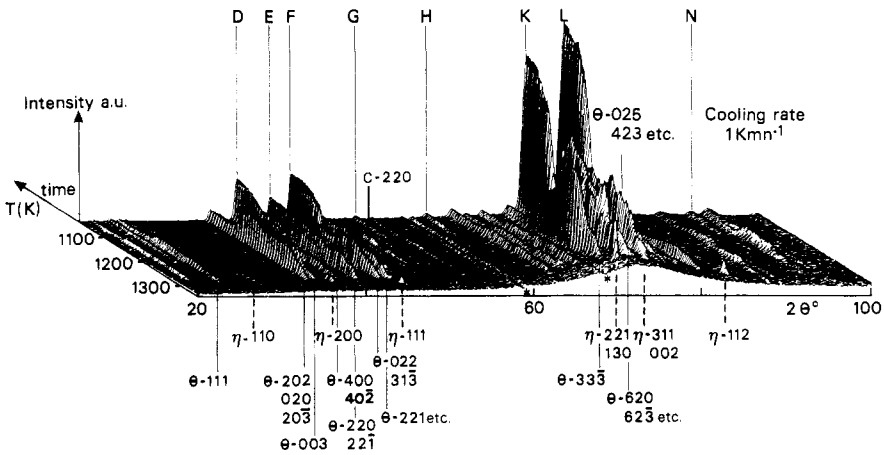

Figure 8. Three-dimensional view of the path from liquid state to solid state upon cooling at a rate of 1 K min^{-1}. The background intensity has been subtracted from each pattern. Two deficient cells of the detector cause the meaningless negative peaks marked by stars. Notation for the I phase is adopted from [10].

state at $T = 1325$ K to solid state at $T = 1070$ K when the icosahedral phase has fully grown (cooling rate = 1 K min^{-1}). A first peritectic reaction takes place at $T_1 = 1304$ K and produces the orthorhombic η-Al_5Fe_2 phase (the η phase) [17] in equilibrium with liquid. This was not expected since it was not observed during the heating process. A possible explanation may be that this peritectic reaction is sensitive to cooling or heating rate, our heating rate of 4.4 K min^{-1} possibly being too rapid for this reaction to occur. The second peritectic reaction begins at $T_2 = 1284$ K, which transforms the η phase plus liquid mixture into the monoclinic θ phase in addition to liquid and the C phase. The existence of texture is seen from comparison of peak intensities with that of an isotropic distribution. Soon afterwards, the C phase appears at 1218 K. It then joins the peritectic reaction at 1134 K when the I phase forms. The growth of the I phase is also completed at about 1070 K (with this cooling rate) but a small quantity of the θ phase is also present. These peritectic reactions are reversible as comparison with the heating process demonstrates.

In order to judge the presence of residual liquid, figure 9 draws the neutron counts versus temperature of the background measured at $2\theta = 68.6$–$68.8°$ where there is no sharp diffraction peak. Accordingly, this intensity is the sum of the incoherent scattering from the whole sample and the coherent scattering from liquid. Each step when a reaction occurs is accompanied by a sudden decrease in the background plot, indicating that liquid is being consumed more rapidly. Four slope changes are seen at the temperatures already mentioned, which correspond to the four peritectic reactions:

$$T_1 = 1304\ \text{K} \qquad \text{L} \rightarrow \text{L} + \eta$$

$$T_2 = 1284\ \text{K} \qquad \text{L} + \eta \rightarrow \text{L} + \theta$$

$$T_3 = 1218\ \text{K} \qquad \text{L} + \theta \rightarrow \text{L} + \theta + \text{C}$$

$$T_4 = 1134\ \text{K} \qquad \text{L} + \theta + \text{C} \rightarrow \text{I} + \theta.$$

The I phase forms in the last peritectic reaction involving phases θ, C and L. An estimate of the L phase volume fraction f_L at each stage may be obtained by assuming that the

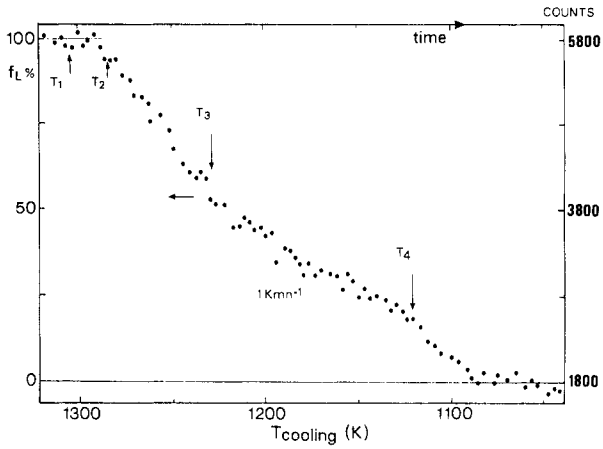

Figure 9. Background intensity measured at $2\theta = 68.6$–$68.8°$ as a function of temperature during cooling from the liquid.

average coherent scattering length of the liquid does not change much over the present temperature range. Then f_L is about 20% as deduced from the linear scale reported in figure 9. In fact composition change is inevitable and this value has only semi-quantitative meaning. Though the quantity of the L phase is very little, liquid is undoubtedly present at the temperature T_4 and makes the formation of the I phase a peritectic reaction. One can also see that, at the end of this reaction, there is almost no L phase present, indicating that the formation of the I phase ends in a solid-state reaction. This detail will be discussed further in this paper after the isothermal growth of the I phase has been analysed.

Upon further cooling, the $\theta + I \rightarrow R + \theta + C$ eutectoid decomposition has not been observed. Since this reaction takes place in the solid state, it may be suppressed under the relatively high cooling rate (14.5 K min^{-1}) that we used within the lower temperature range. The sensitivity on cooling rate may explain the controversies concerning the perfection of the Al–Cu–Fe icosahedral phase obtained under rather similar solidification conditions [7, 10, 16, 18]. The key element to obtain the perfect I phase is to avoid the formation of the R phase by quick cooling in the temperature range around and below 910 K.

4.3. Discussion

The heating and cooling processes are almost reversible except for the two transformations: $L \rightarrow L + \eta$ and $R + \theta + C \rightarrow I + \theta$. We attribute their respective absence upon heating and cooling to the use of relatively high heating or cooling rates. One obvious fact is that the θ phase is involved in almost all the phase transformations. It appears that this phase plays an important role in the phase transformations concerning the I phase. The θ-$Al_{13}Fe_4$ phase has been found to be the decomposition product of the Al–Fe decagonal phase [19]. From the crystallographic point of view, it has a very close relationship with quasi-crystals because one can find many icosahedral subunits that can also be the basic structure of quasi-crystals. In the present case, the I phase becomes the decomposition product of the θ phase, despite the fact that involvement of phases C and L complicates the explanation of this transformation process. However, it is worth

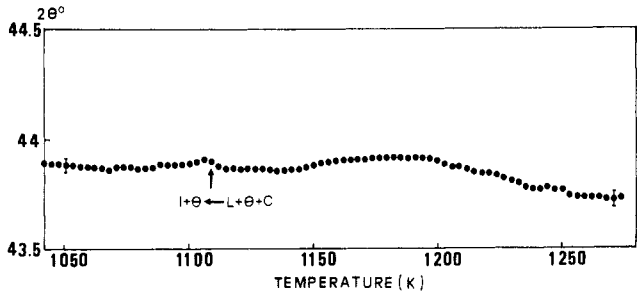

Figure 10. Position of the $(022, 31\bar{3})$ peak of the θ phase as a function of temperature during cooling from liquid state under cooling rate of 1 K min^{-1}. The arrow marks the point when the I phase begins to grow.

examining the behaviour of the θ phase in order to see why it is less stable than the I phase upon cooling down and to study which factor dominates this process. Referring back to figures 4 and 8, in which the perspective views of heating and cooling are shown, we can see that the Bragg peak intensities of the θ phase do not change uniformly. For instance, the θ-(003) peak undergoes an intensity change much greater than that of the θ-$(202, 20\bar{3}, 020)$ group of peaks at the transition, the former peaks being abnormally strong and the latter being abnormally weak with reference to the ratio expected for an isotropic powder sample of the θ phase at high temperature.

In contrast, the low-temperature pattern does not show a significant departure from isotropic distribution. A waving shift of the interplanar distances as a function of decreasing temperature (see figure 10, which presents as an example the position of a Bragg peak in 2θ space) is also suggestive of some precursor rearrangements in the monoclinic lattice taking place before the transformation proceeds. We can reasonably assign this effect to a higher solubility of Cu into the θ phase structure at high temperature. Reducing the temperature also largely decreases the Cu solubility. In fact the solubility of Cu at room temperature is only about 5 at.% according to x-ray spectroscopy composition analysis of the residual θ phase [2]. Thus the instability of the θ phase at lower temperature is caused by the addition of copper and the transformation in turn may be controlled by copper diffusion. This point will be further discussed in the next section.

The C phase structure is still largely unknown. We have obtained its BCC lattice constant (a = 8.28 Å) from a fit of the neutron diffraction pattern taken at 4 K. Though the volume fraction of this phase is rather small, its influence on the I phase formation seems important: whenever the I phase grows, the C phase disappears. The abundance of the C phase during heating can be traced by its (220) peak as shown in figure 4. Further investigation is needed to understand fully its relation with the I phase.

5. Isothermal growth of the icosahedral phase

5.1. Experimental results

According to the cooling experiment discussed above, which reveals that the I phase forms in a peritectic reaction involving phases θ, C and L in the temperature range between 1134 and 1070 K, a heat treatment scheme was chosen (figure 11) in order to drive the isothermal growth of the I phase and to verify its reversibility. This scheme

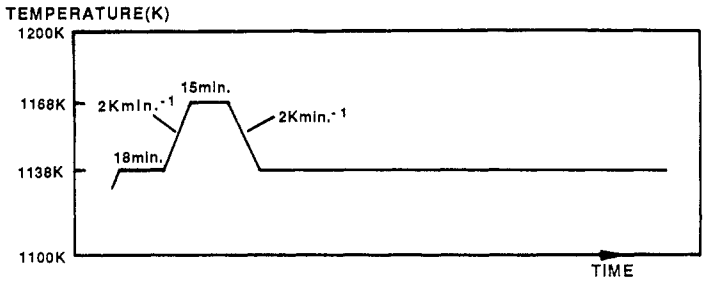

Figure 11. Heat treatment scheme adopted in the present investigation. Isothermal growth of the I phase is realised during the annealing at 1138 K for 3 h.

consists first in maintaining an ingot at 1138 K for a short time, then heating up to 1168 K, quickly cooling again to 1138 K and at last annealing at this temperature for 3 h. Figure 12 is the 3D perspective view of this process as recorded by neutron diffraction at 3 min intervals. The I phase tends to disappear whereas phases θ and C tend to increase as the temperature is raised to 1168 K and then, during annealing at 1138 K, the I phase grows again isothermally at the expense of phases θ and C. At last the C phase is consumed completely. Judging the degree of reversibility is straightforward. Such a process is more clearly shown by comparing intensities of peak D of the I phase and peak (202, $20\bar{3}$, 020) of the θ phase during the growth of the I phase (figure 13). There are two remarkable features concerning these two curves. First, at the beginning of the transformation, the former intensity rises much faster than the latter, i.e. the growth rate of the I phase is much quicker than the decomposition rate of the θ phase. This implies that there exist

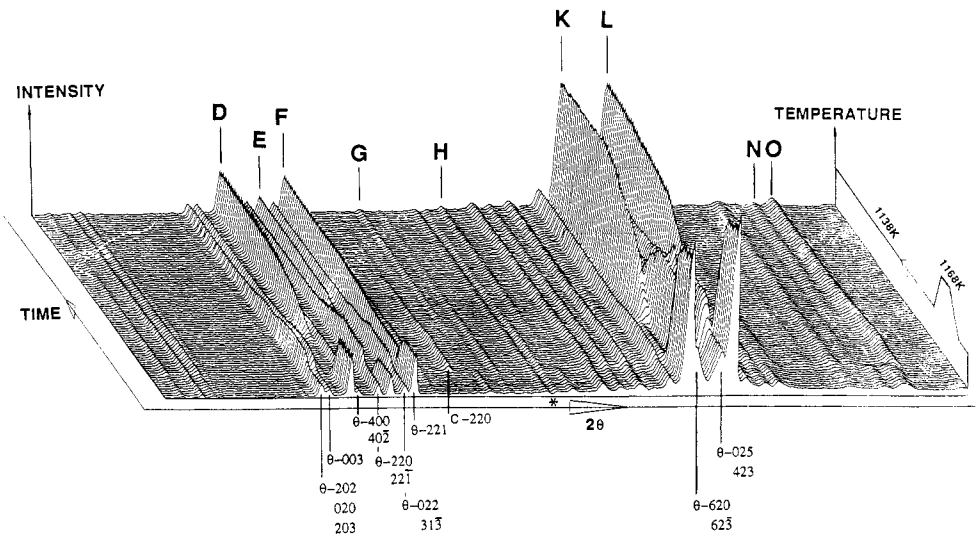

Figure 12. Three-dimensional view recorded by neutron diffraction at 3 min intervals. The heat treatment scheme of figure 11 is drawn on the right side for the sake of comparison. The I phase disappears upon heating up to 1168 K and regrows during annealing at 1138 K. It is also noted that the intensities of peaks (202, $20\bar{3}$, 020) and (003) of the θ phase change in different ways during the whole process (see figures 4 and 8). One deficient cell of the detector causes the meaningless negative peak marked by a star.

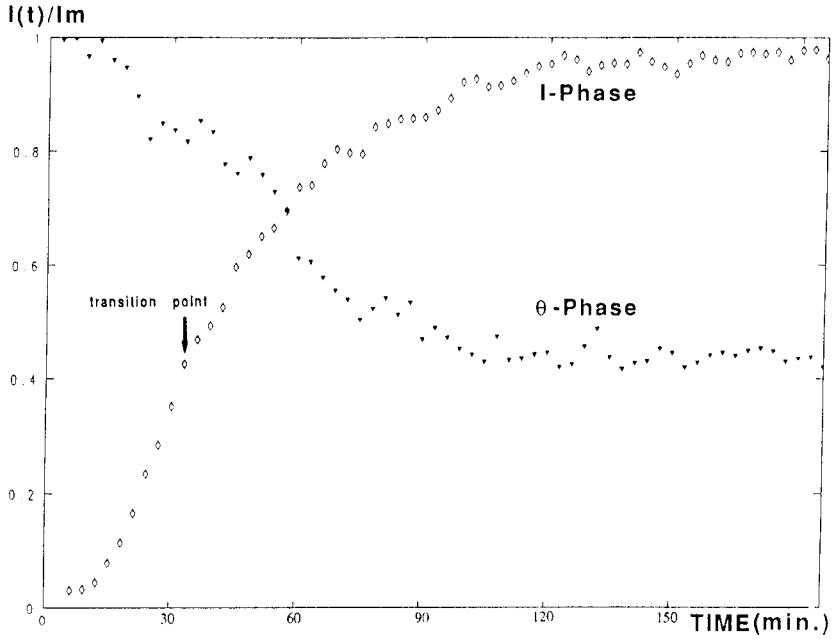

Figure 13. Intensities of the D peak of the I phase and of the $(202, 20\bar{3}, 020)$ peaks of the θ phase as functions of time during annealing at 1138 K. The ratio of the intensity at time t $(I(t))$ to the maximum intensity (I_m) is taken as the Y axis. The transition point from the first stage to the second one is marked by an arrow.

other phases contributing to the formation of the I phase. The possible candidates are phases C and L. Secondly, at the second stage, the rise of the I phase curve and the fall of the θ phase curve behave in a complementary way, i.e. the growth rate of the I phase and decomposition rate of the θ phase are the same. At this time, the C phase has already disappeared. Actually this indicates a solid-phase reaction where the θ phase transforms to the I phase directly. This specific point is labelled 'transition point' in figure 14. Such a phenomenon is the same as in the case of continuous cooling. The half transforming time $t_{1/2}$, which is a parameter to catalogue the reaction speed, approximately equals 40 min, and can be easily calculated from the curve of the I phase.

The L phase fraction is deduced from the plot of background intensity against time measured as in the previous section at the $2\theta = 68.6$–$68.8°$ position (figure 14). The heating up to 1168 K is accompanied by a rise of the liquid background, and therefore the I phase is replaced by phases L, θ and C; the 1138 K annealing begins with the state of phases L plus θ and C and ends with I plus θ. Thus the first stage of reaction involving phases I, θ, C and L is of the peritectic type. If the composition change during cooling and annealing is ignored so that the average coherent scattering length of the liquid does not change dramatically, the L phase fraction f_L is estimated to be about 10% at the beginning of the reaction. In fact, this is rather arbitrary because a composition change is inevitable. After consumption of phases L and C, the reaction proceeds to another stage in the solid state where the θ phase transforms to the I phase directly. Thus the formation of the I phase is in two stages: the first is a peritectic reaction and the second a solid-state one.

Coincidentally, the peak intensities of the θ phase do not change uniformly. For example, in figure 15, the intensity of the $(202, 20\bar{3}, 020)$ peak is higher than that of

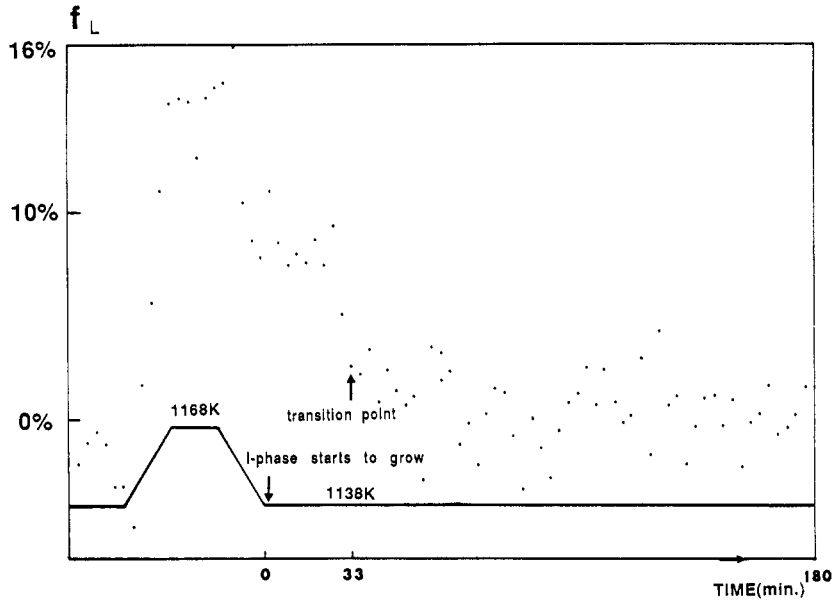

Figure 14. Background intensity scattered by the liquid phase versus time as measured at position $2\theta = 68.6$–$68.8°$. When the second stage of growth begins, there is almost no more liquid. The transition point is marked by an arrow.

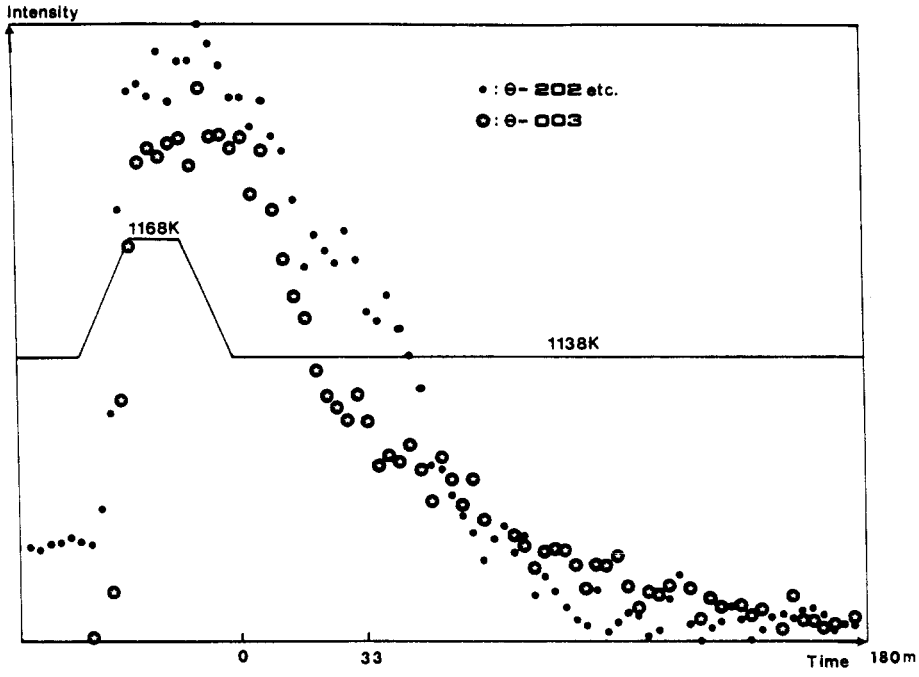

Figure 15. Intensities of peaks $(202, 20\bar{3}, 020)$ and (003) of the θ phase as functions of time. The heat treatment scheme is also presented as a reference.

the (003) peak at 1168 K and at the beginning of the 1138 K annealing, while, as the I phase grows, the latter becomes higher. This behaviour is comparable to the one already described above, suggesting that copper diffusion is also associated with the isothermal growth of the I phase. Thus the transfer of Cu from the θ phase to the I phase plays an important role in the decomposition of the θ phase and the formation of the I phase.

5.2. *Discussion on the isothermal transformation curve*

Generally the isothermal transformation curve can be expressed by an Avrami equation,

$$\zeta = 1 - \exp(-kt^n) \tag{1}$$

where ζ represents the volume fraction transformed at time t, k is the rate constant, and n is supposed to be related to the transformation mechanism. Therefore, a $\log\{\log[1/(1-\zeta)]\}$ versus $\log(t)$ curve may be drawn on the assumption that

$$\zeta = I(t)/I_m \tag{2}$$

where $I(t)$ is the integrated intensity of individual peaks as a function of time starting from the appearance of the I phase and I_m is the maximum value of $I(t)$. Though all the peaks show the same trend (the texture of the I phase is not observable), peak D of the I phase is chosen because it has a fairly high intensity and is well apart from peaks nearby. As shown in figure 16, this curve consists of two linear parts with slope rates $n_1 = 2.5$ and $n_2 = 1.3$ respectively. It follows that two Avrami equations can be obtained,

$$\zeta = 1 - \exp(-9.05 \times 10^{-5} t^{2.5}) \qquad t = 12\text{–}33 \text{ min} \tag{3}$$

$$\zeta = 1 - \exp(-6.01 \times 10^{-3} t^{1.3}) \qquad t = 33\text{–}141 \text{ min}. \tag{4}$$

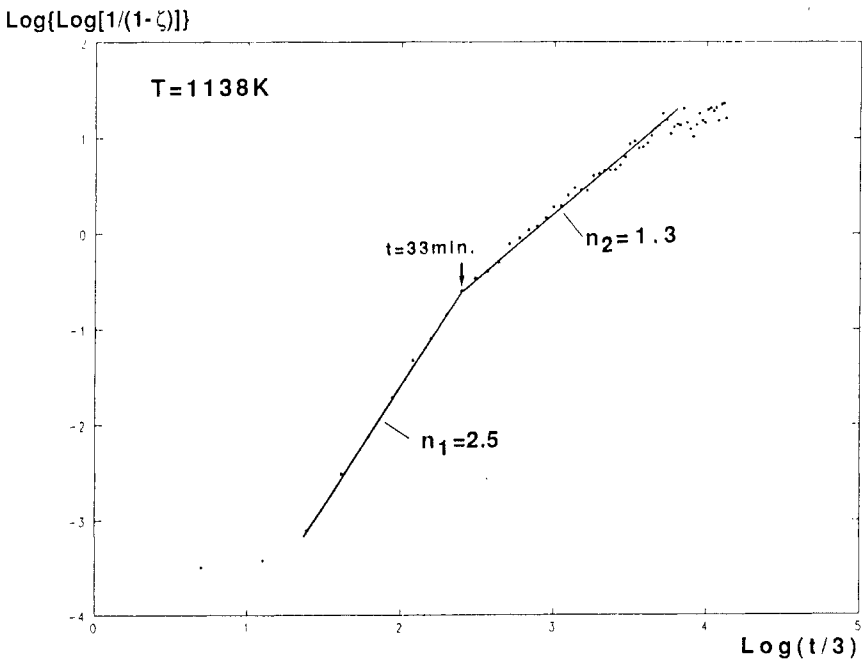

Figure 16. $\log\{\log[1/(1-\zeta)]\}$ versus $\log(t)$ plot of the D peak intensity of the I phase showing two stages of growth.

Table 2. Some features of the two-stage growth of the I phase at 1138 K.

	First stage	Second stage
Lasting time	20 min	110 min
Phases present	L, θ, C, I	θ, I
Type of reaction	L + θ + C → I + θ (peritectic)	θ → I (solid-state)
FWHM	Decreasing	Change is equal to or smaller than the experimental resolution (0.41° in 2θ scale)
n value in Avrami equation	2.5	1.3
Suggested mechanism	Diffusion-controlled	Nucleation-site saturation

According to Christian [20], $n = 5/2$ corresponds to a diffusion-controlled reaction with constant nucleation rate. This seems to confirm the above assumption of a Cu diffusion process associated with the growth of the I phase. At this stage there is a peritectic reaction schematised by the equation L + θ + C → I + θ (figure 14). As the liquid fraction is very small, it is conceivable that the remaining liquid is in grain boundaries forming a liquid boundary network. The diffusion takes place preferentially through this liquid boundary. The transition to the next linear part is suggested to be due to nucleation-site saturation [21], which starts at the moment when the liquid is almost consumed, as is easily seen in figure 14. Christian [20] also suggested that after randomly distributed nucleation sites are saturated, the n value is 1.5, close to our value of $n = 1.3$.

To sum up, the analysis of the isothermal growth of the I phase has led to the determination of some quantitative parameters concerning the two-stage growth of the I phase. These results are listed in table 2 where the features of the two-stage growth are compared. In short, the formation of the I phase begins with a peritectic reaction L + θ + C → I + θ and ends with the solid-state reaction θ → I, and the growth of the I phase is diffusion-controlled.

6. Run 2: heating process of the $Al_{65}Cu_{20}Fe_{15}$ melt-spun sample

6.1. Experimental results

For the sake of comparison with the ingot sample obtained by conventional solidification, a heating process monitored with a heating rate of 1 K min^{-1} was performed on powders prepared from melt-spun ribbons of nominal composition $Al_{65}Cu_{20}Fe_{15}$. In the as-quenched state, three phases can be identified, namely the I phase, Al_2Cu [22] and Al_7Cu_2Fe [23] (figure 17). The I phase is also of the 6D FCC type, as in the case of the ingot sample. Previously Ebalard and Spaepen [24] have found the same results. The main coexisting crystalline phase is the Al_2Cu phase. Only the (215) and (321, 305) peaks of the Al_7Cu_2Fe phase (T phase) are observed, and thus its amount must be very little. The development of these peaks upon heating has been traced to ensure that they belong to the T phase.

During heating up to the liquid state, the sample undergoes a series of phase transformations as revealed by the contour plot in figure 18. From room temperature to T_1 = 690 K, there is no change in the sample. Between T_1 and T_2 = 740 K the first phase

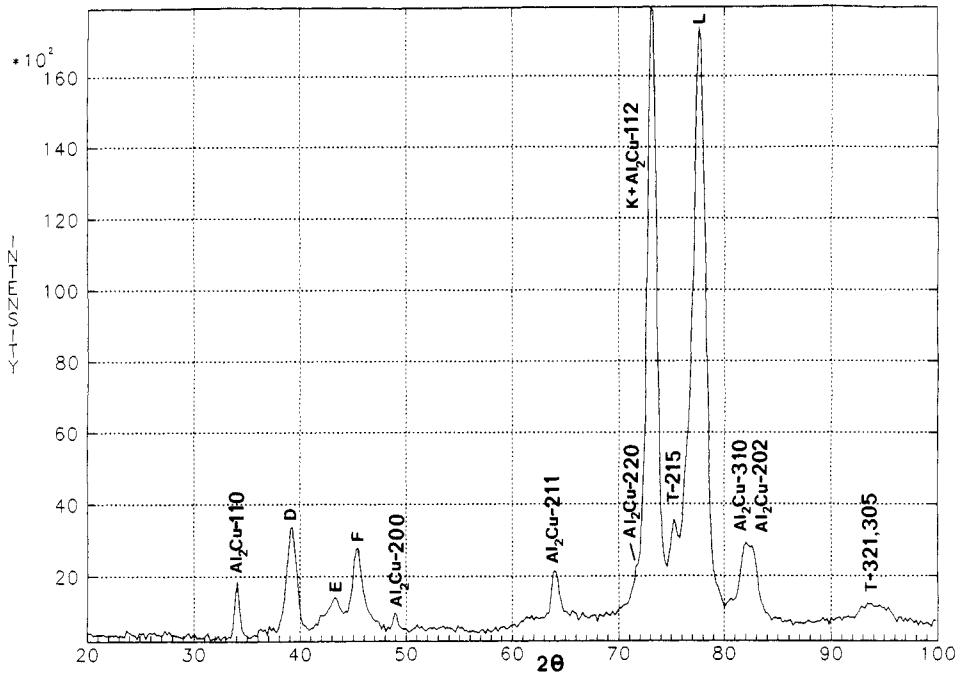

Figure 17. Neutron diffraction pattern of the melt-spun powder sample in the as-quenched state at room temperature.

transformation occurs: the Al_2Cu peaks begin to disappear, the I phase peaks fall rapidly and, as a consequence, those of the T phase augment, which suggests a eutectoid reaction: $I + Al_2Cu \rightarrow I + T$. T_1 is much lower than the melting point of the pure Al_2Cu phase (roughly 900 K [22]). Right afterwards, the T phase peaks increase gradually at the expense of the consumption of the I phase until $T_3 = 877$ K when the reverse process starts, i.e. the I phase grows again while the T phase is consumed. Figure 19 is the neutron diffractogram showing the coexistence of phases I and T at 980 K. Note also the characteristic behaviour of peak E. Its intensity change is the signature of an $F \rightarrow P$ transition in 6D cubic real space, which will be discussed later. At $T_4 = 1025$ K the T phase disappears completely, followed by a peritectic reaction that transforms the I phase into the θ-$Al_{13}Fe_4$ phase plus the L and C phase mixture according to the formula: $T + I \rightarrow \theta + L + C$. This is in agreement with the experiment on the ingot sample discussed above. This peritectic reaction is finished at $T_5 = 1085$ K, when the last peritectic reaction, $C + \theta + L \rightarrow L$, takes place. Finally at temperatures higher than $T_6 = 1273$ K, the θ phase completely melts into liquid.

The last two reactions almost repeat what has been found with the ingot sample except that the C phase and the θ phase disappear together. But temperatures T_5 and T_6 are considerably below the corresponding temperatures characteristic of the ingot sample (1165 and 1317 K upon heating, 1134 and 1284 K upon cooling, respectively). The effect of heating rate may contribute to this difference since the heating rate here (1 K min^{-1}) is much slower than those used with the ingot sample (more than 4 K min^{-1}, see table 2), but it cannot explain why T_5 and T_6 are even lower than the corresponding temperatures upon cooling. This may indicate that the compositions of these two samples

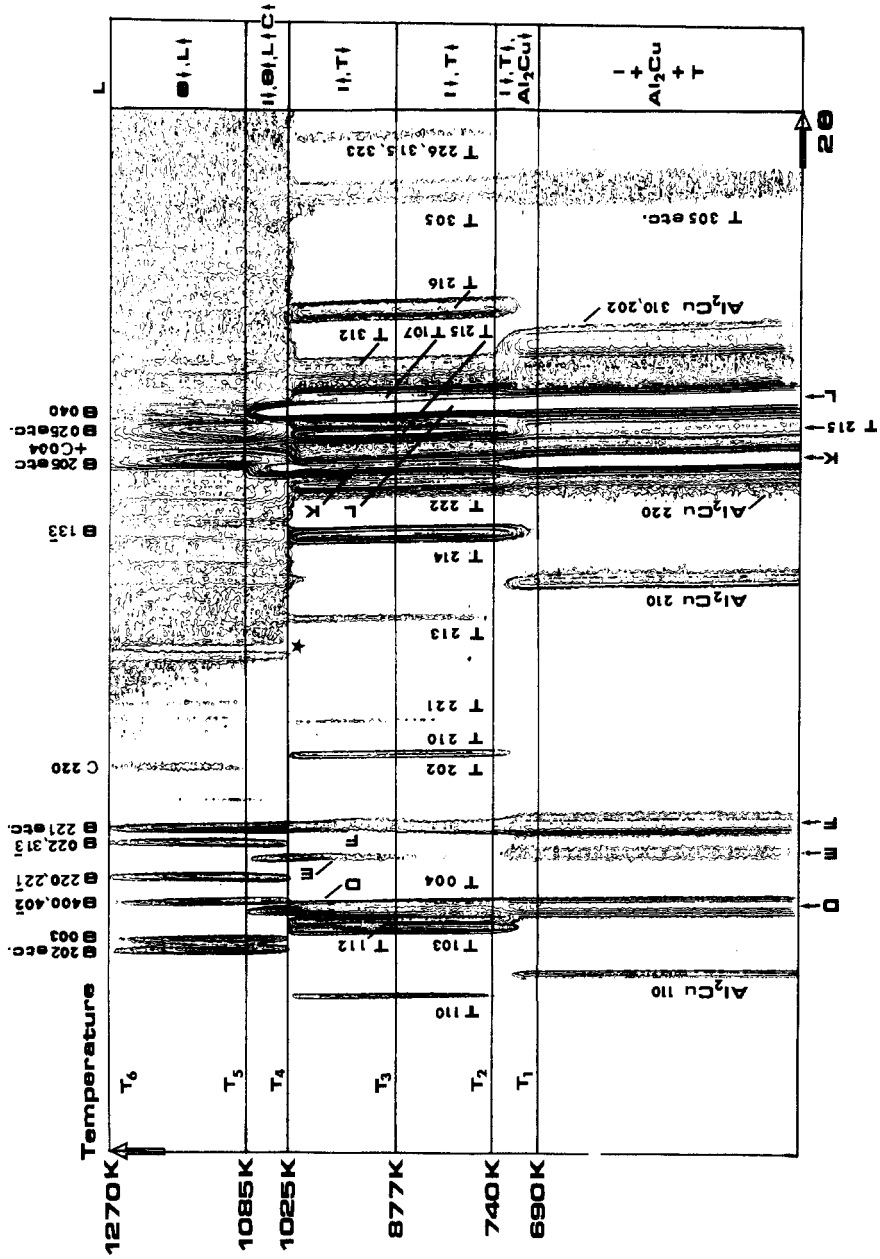

Figure 18. Contour plot of the development of neutron diffraction patterns showing the heating process of melt-spun sample from room temperature to the liquid state with a heating rate of 1 K min^{-1}. Notice that this contour plot does not show precisely when the intensities start to decrease. The temperatures determined from the temperature evolution of integrated intensities are used in the text to define the transition temperature reported on the left-hand axis.

are slightly different. The transformation temperatures may be sensitive to the location of composition in the Al–Cu–Fe system. One can expect that the boundary lines separating the L/L + θ + C and L + θ + C/L + I + θ phase zones in the schematic phase diagram as proposed on the basis of the cooling process (figure 7, [2]) have steep curves.

6.2. *Discussion*

The as-quenched state of our sample is basically the same as what Tsai *et al* [25] have obtained except for the existence of a small amount of the T phase in our melt-spun sample. Upon heating, no sudden change of the peak amplitude is observed, which would indicate the R → I phase transformation, so that what is quenched at room temperature by melt-spinning is the I phase.

The T phase is the only stable crystalline phase known in the vicinity of the I phase composition of $Al_{63.5}Cu_{24}Fe_{12.5}$. It has a tetragonal cell with $a = 6.33$ Å, $c = 14.81$ Å, and its exact formula is $Al_{70}Cu_{20}Fe_{10}$ [23], containing an Al content about 10 at.% richer than that of the I phase while the relative content of Cu and Fe is almost the same. So far, there has not been any direct evidence that the T phase is linked with the I phase transformations. Within the temperature range between 690 and 1025 K, we clearly see that this phase is involved in the reactions concerning the I phase; especially between 740 and 1025 K, there exist mutual transitions between phases T and I. Figure 19 is the neutron diffraction pattern taken at 980 K when the T → I reaction proceeds, from which the lattice parameters of $a = 6.41$ Å, $c = 15.01$ Å, or roughly 1.3% larger than those at room temperature, can be obtained. Comparing figure 19 with the calculated

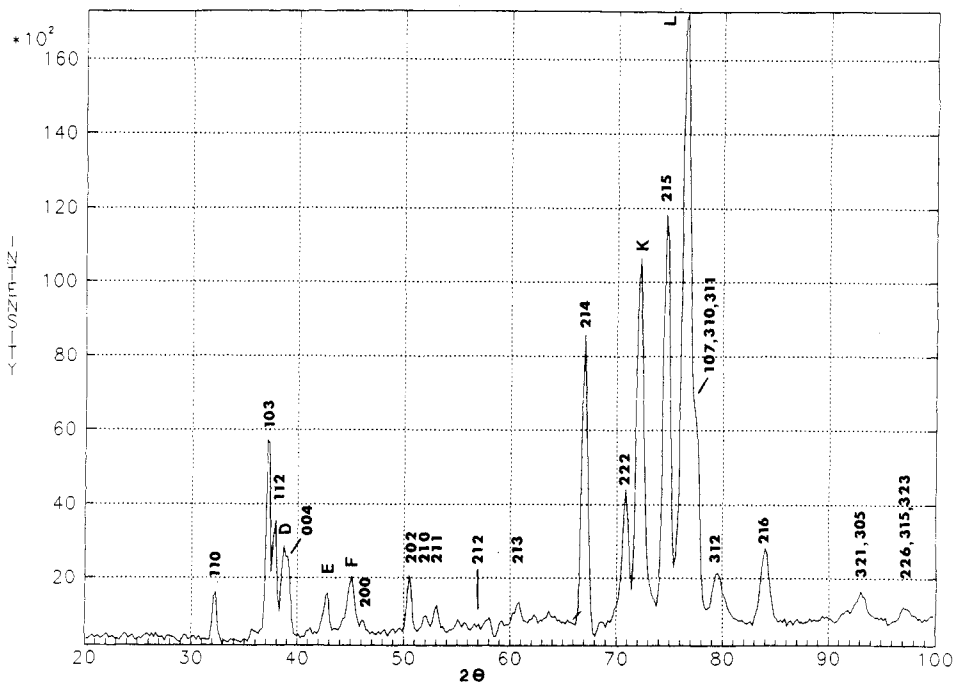

Figure 19. Neutron diffraction pattern taken at 980 K showing the coexistence of phases I and T.

intensity distribution based on the atomic position data proposed for the ideal T phase [23], we can find that the (212) peak with theoretical intensity of 52 (intensity of the most intense peak being 100) does not appear in the experimental pattern while the (214) peak with the experimental value of 58 is abnormally high compared to the theoretical intensity of 7. Since the other peaks do not show significant departure from the theoretical calculation, this cannot be caused by any texture effect. As already mentioned above, the T phase has an Al content about 10 at.% richer than that of the I phase. Thus we suspect that the composition of the T phase at this temperature is different from that at room temperature. It is reasonable to assume that this change must approach the composition of the I phase. To solve this question, simulated diffraction patterns were calculated for different sets of atomic locations on the crystallographic sites of the T phase. As a primary trial, four Al positions with unit-cell coordination of $(0, 0, Z_1)$ are replaced by four Fe atoms, so that the resultant composition of the T phase is now $Al_{60}Cu_{20}Fe_{20}$. Because the difference between neutron coherent scattering lengths of the Fe ($0.954\ cm^{-12}$) and Cu ($0.769\ cm^{-12}$) atoms is small compared to the one with the Al atom ($0.345\ cm^{-12}$), we can expect that the adjustment of relative content of Cu and Fe, for example $Al_{60}Cu_{25}Fe_{15}$, will not greatly affect this intensity distribution. Not to our surprise, the (212) peak intensity is reduced to 0.1, too small to be observed experimentally, while the (214) peak intensity is increased to 61, very close to the observed intensity 58. The pattern thus obtained shows a much better agreement with the experimental one in figure 19. Therefore, it seems certain that the T phase at high temperature has a composition much closer to that of the I phase than at room temperature. During I ↔ T mutual transition, the irregular change of peak intensities or positions, as is observed in the $\theta + L + C \rightarrow I + L$ phase transformation in the ingot sample, is not present. This may imply that there is little or no elemental transfer associated with the I ↔ T transformation. Accordingly we conclude that the I ↔ T phase transformations are interface-controlled. The existence of a critical point T_3, when the I → T transition is reversed, suggests that their relative stability depends on temperature.

It is also interesting to note that, above $T_2 = 740$ K, though all the I phase peaks begin to fall, peak E decreases faster than the other peaks of the I phase, e.g. the L peak (note that the K peak also shows an irregular fall, which is caused by the disappearance of the overlapping (220) peak of the Al_2Cu phase). The E peak is too weak to be visible in the contour plot of figure 18 before the critical temperature T_3 is reached. Beginning from T_3, a reverse process occurs, the E peak rises faster. As peak E originates from the FCC type of the I phase (see table 1), its intensity change reflects the degree of FCC ordering accompanying the I phase transformations. From T_2 to T_3, this ordering is weakened; above the critical point T_3, the FCC ordering is reinforced again. The peak height ratios of the D and E peaks at room temperature, T_2 and T_4 are calculated to be 3, 4 and 2 respectively. Larger values correspond to weaker FCC ordering, so that from room temperature to T_4 the FCC ordering undergoes a weakening → reinforcing process; at T_4, the I phase is even better ordered than at room temperature. Thus, the I phase passes successively through an F → P disordering and a P → F ordering transition within the temperature ranges from T_1 to T_4. Though sometimes the FCC feature is very weak, it is always kept during the whole heating process. But even the smallest value is still larger than that of the ingot sample after heat treatment (where this ratio is about 1.5), indicating that the I phase from rapid solidification has a much weaker FCC ordering than the I phase from slow solidification. Ebalard and Spaepen [24] have observed P → F transition upon heating melt-spun Al–Cu–Mn/Cr alloys, but they failed to detect any change of FCC ordering upon heating Al–Cu–Fe melt-spun ribbons.

Moreover, the I phase produced by melt-spinning has much broader peak widths. So the melt-spun I phase has more structural faults than that obtained by slow solidification. For peak K, the FWHM is about 1° in 2θ scale, or 51 nm^{-1} in Q scale, in sharp contrast to the value of 0.8° or 40 nm^{-1} of the I phase in the ingot sample after heat treatment. This is in quantitative agreement with previous results [26]. The FWHM is significantly reduced at high temperature. It is natural that heating improves the structural perfection, which may include the disappearance of antiphase domains [9, 24]. However, this does not mean that the FCC ordering is also enforced. It seems that the structural perfection and FCC ordering are two separate processes.

At temperatures higher than T_4, two peritectic decompositions with formulae $I + L \rightarrow \theta + L$ and $\theta + L \rightarrow L$ take place successively, which have been well examined in the ingot sample.

In short, upon heating from room temperature to the melting point, the $Al_{65}Cu_{20}Fe_{15}$ melt-spun sample undergoes the following phase transformations:

$$T_1 = 690\ K \qquad I + Al_2Cu \rightarrow T$$
$$T_2 = 740\ K \qquad I \rightarrow T$$
$$T_3 = 877\ K \qquad T \rightarrow I$$
$$T_4 = 1025\ K \qquad I \rightarrow \theta + L + C$$
$$T_5 = 1085\ K \qquad \theta + L + C \rightarrow L.$$

7. Conclusions

An overview of the phase transformations taking place in the $Al_{65}Cu_{20}Fe_{15}$ ingot sample during heating and cooling is shown in table 3. All the continuous heating, cooling and isothermal annealing processes show that the I phase forms (or decomposes) in a peritectic reaction involving phases L, C and θ. Detailed analysis of the isothermal growth of the I phase during cooling reveals that its growth proceeds in two stages. The first one is characterised by the presence of the L phase so that the reaction is peritectic: $L + \theta + C \rightarrow I + \theta$. The second one is a reaction in solid state: $\theta \rightarrow I$. This reaction is preceded by two other peritectic reactions, $L \rightarrow L + \eta$, $L + \eta \rightarrow L + \theta$, and is probably followed by a solid-state peritectoid reaction, $I + \theta \rightarrow R + C + \theta$ (from the perfect I

Table 3. An overview of the heating and cooling processes of the $Al_{65}Cu_{20}Fe_{15}$ ingot.

Heating rate (K min^{-1})	2.6	4.3	4.4
Temperature (K)	910→	1117→1165	→1250
Heating	$R + \theta + C \rightarrow I + \theta$	$I + \theta \rightarrow L + C + \theta$	$L + C + \theta \rightarrow L + \theta$
Cooling		$I + \theta \leftarrow L + C + \theta$	$L + C + \theta \leftarrow L + \theta$
Temperature (K)		←1134	←1218
Cooling rate (K min^{-1})	14.5	1	1
Heating rate (K min^{-1})	4.4	4.4	
Temperature (K)	→1317		
Heating	$L + \theta \rightarrow L$		
Cooling	$L + \theta \leftarrow L + \eta$	$L + \eta \leftarrow L$	
Temperature (K)	←1284	←1304	
Cooling rate (K min^{-1})	1	1	

phase to the microcrystalline R phase), if the cooling rate is sufficiently slow. This also means that the perfect I phase is not a truly equilibrium phase at room temperature. The growth of the I phase is diffusion-controlled. The enhanced solubility of Cu into the θ phase at high temperature may be responsible for the decomposition of the θ phase to the I phase upon cooling.

In the case of the melt-spun sample, the T phase has been found to be involved directly in the transformations concerning the I phase. Its composition at high temperature is supposed to be close to that of the I phase. The I phase at temperatures above 740 K has a much more perfect structure than in its as-quenched state, but the FCC ordering goes through a weakening and reinforcing process upon heating. The I phase produced by rapid solidification corresponds to the I phase found in the ingot sample, though its FCC ordering is weaker. The I phase is decomposed in the same way as in the case of the ingot sample upon heating.

Acknowledgments

The Institut Laue Langevin is gratefully acknowledged for the allocation of beam time and for the provision of financial support to two of us (CD and M de B). We thank J P Houin for his assistance during sample preparation. We are deeply indebted to Dr J Pannetier for his help during the experiment and for most fruitful discussions.

References

[1] Tsai A P, Inoue A and Masumoto T 1987 *Japan. J. Appl. Phys.* **26** L1505
[2] Dong C, de Boissieu M, Dubois J M, Pannetier J and Janot C 1989 *J. Mater. Sci. Lett.* **8** 827
[3] Dubost B, Lang J M, Tanaka M, Sainfort P and Audier M 1986 *Nature* **324** 48
[4] Lang J M, Audier M, Dubost B and Sainfort P 1987 *J. Cryst. Growth* **83** 456
[5] Steinhardt P J and Ostlund S 1987 *The Physics of Quasicrystals* (Singapore: World Scientific) p 292
[6] Audier M and Guyot P 1989 *Quasicrystals and Incommensurate Structures in Condensed Matter* ed M J Yacaman, D Romen, V Castano and A Gomez (Singapore: World Scientific) p 288
[7] Ebalard S and Spaepen F 1989 *J. Mater. Res.* **4** 39
[8] Cahn J W, Shechtman D and Gratias D 1986 *J. Mater. Res.* **1** 13
[9] Devaud-Rzepski J, Quivy A, Calvayrac Y, Cornier-Quiquandon M and Gratias D 1989 *Phil. Mag.* B **606** 855
[10] Ishimasa T, Fukano Y and Tsuchimori M 1988 *Phil. Mag. Lett.* **583** 157
[11] Audier M and Guyot P 1989 *Adriatico Research Conf. on Quasicrystals, Trieste* ed M Jaric (Singapore: World Scientific) p 156
[12] Dénoyer F, Heger G, Lambert M, Audier M and Guyot P 1990 *J. Physique* **51** 651
[13] Audier M, de Boissieu M, Dubois J M and Janot C 1990 *Phys. Rev. Lett.* submitted
[14] Pannetier J, Dubois J M, Janot C and Bilde A 1987 *Phil. Mag.* B **55** 435
[15] Black P J 1955 *Acta Crystallogr.* **8** 43
[16] Hiraga K, Zhang B P, Hirabayashi M, Inoue A and Masumoto T 1988 *Japan. J. Appl. Phys.* **27** L951
[17] Schubert K, Rosler V, Kluge M, Anderko K and Harle L 1953 *Naturwissenschaften* **16** 437
[18] He L X, Wu Y K and Kuo K H 1988 *J. Mater. Lett.* **7** 1284, 1286
[19] Fung K K, Zou X D and Yang C Y 1987 *Phil. Mag. Lett.* **551** 27
[20] Christian J W 1965 *Physical Metallurgy* ed R W Cahn (Amsterdam: North-Holland)
[21] Cahn J W 1956 *Acta Metallurg.* **4** 449
[22] Pantasis A and Walchtal E 1978 *Z. Metallkd.* **69** 50
[23] Bown M G and Brown P J 1956 *Acta Crystallogr.* **9** 911
[24] Ebalard S and Spaepen F 1990 *J. Mater. Res.* **5** 62
[25] Tsai A P, Inoue A and Masumoto T 1987 *J. Mater. Sci. Lett.* **6** 1403
[26] Tsai A P, Inoue A and Masumoto T 1989 *J. Mater. Sci. Lett.* **8** 470